Physica Scripta. Vol. T80, 220–222, 1999

Improved Dynamic Simulation of Highly Charged Ion–Surface Collisions

J. Ducrée,[1*] H. J. Andrä[1] and U. Thumm[2]

[1] Institut für Kernphysik, Westfälische Wilhelms-Universität Münster, Wilhelm-Klemm-Str. 9, D-48149 Münster, Germany
[2] J. R. Macdonald Laboratory, Department of Physics, Kansas State University, Manhattan, Kansas 66506-2604, USA

Received September 14, 1998; accepted in revised form October 6, 1998

PACS Ref: 34.50.Dy, 34.70.+e, 79.20.Rf

Abstract

On the basis of a refined classical overbarrier model, we simulate the evolution of level occupations of slow highly charged ions (HCIs) reflected by metal surfaces. Our calculation includes the full trajectory of the projectile and incorporates atomic structure calculations which provide accurate asymptotic projectile energy levels. We scrutinize effects related to proposed interaction mechanisms, such as peeling off atomic Rydberg levels and small-distance side feeding from the target valence band to inner projectile shells. The *simultaneous* evaluation of projectile energy gains, final charge state distributions, and the emission of projectile Auger electrons agrees well with experiments.

The formation of ions with highly inverted electronic level population, so–called *hollow ions*, near surfaces has attracted increasing interest in the past decade [1,2,3]. Due to their large amount of potential energy, beams of HCIs may find novel applications in the controlled modification of solid surfaces [4,5].

Typically, several 10 atomic units (a.u.) in front of the surface, the effective potential barrier between the ion and the target drops below the work function of the surface and an efficient neutralization via resonant electron capture (RC) sets in. The reverse mechanism, resonant loss (RL), is usually much less efficient and becomes possible when the potential barrier has moved below empty band levels that are degenerate with previously filled projectile levels. The swift charge exchange combined with an intra-atomic autoionization (AI) cascade leads to multiply excited projectiles at intermediate distances from the surface.

The simulations of charge transfer (RC and RL) in this article are based on the classical overbarrier model (COM) [6]. Supplementing our former work [7], we employ a Monte-Carlo sampling to include various projectile Auger-relaxation cascades. Hartree–Fock ionic structure calculations based on the 'Cowan' code [8] are used to obtain asymptotic projectile binding energies E_n. As the HCI approaches the surface these levels are continuously shifted by the classical image potential and changing level occupations.

In Fig. 1, we display the time evolution of RC along a full projectile trajectory for N^{6+} scattering under an incidence angle $\Theta = 45°$ with $E_{kin} = 70$ eV off an Al(111) crystal. All following diagrams will also refer to this collision system. The horizontal axis marks successive RC steps. The two upper graphs show the participating RC level and the corresponding distance from the first lattice layer with their respective statistical spread. The probability for the occurrence of a particular RC step is shown in the bottom graph.

According to the diagram, RC initiates at a distance $R \simeq 22$ a.u. above the surface into the $n = 8$ level. At the sixth RC event at $R \simeq 13$ a.u. (into the $n \simeq 7$ manifold), the HCI is completely neutralized. In order to compensate subsequent electron loss via RL and continuum promotion (CP), RC still continues. Approximately 15 electrons are transfered to the entire ensemble of incident particles and about 25 RC steps are simulated for 50% of the projectiles.

For the low beam energies considered in this work, projectiles transiently plunge into the outskirts of the electron gas before reflection. The drastic change in the dielectric surrounding fuels inner-shell "side feeding" (SF) and loosely bound electrons are "peeled off" (PO) [9]. The stripped-off population is swiftly replaced by an induced charge cloud and inner HCI levels are significantly elevated due to the more compact screening [10,11]. A fast SF mechanism is necessary to explain the high degree of L-shell filling and neutrality among reflected particles [12,13]. On the other

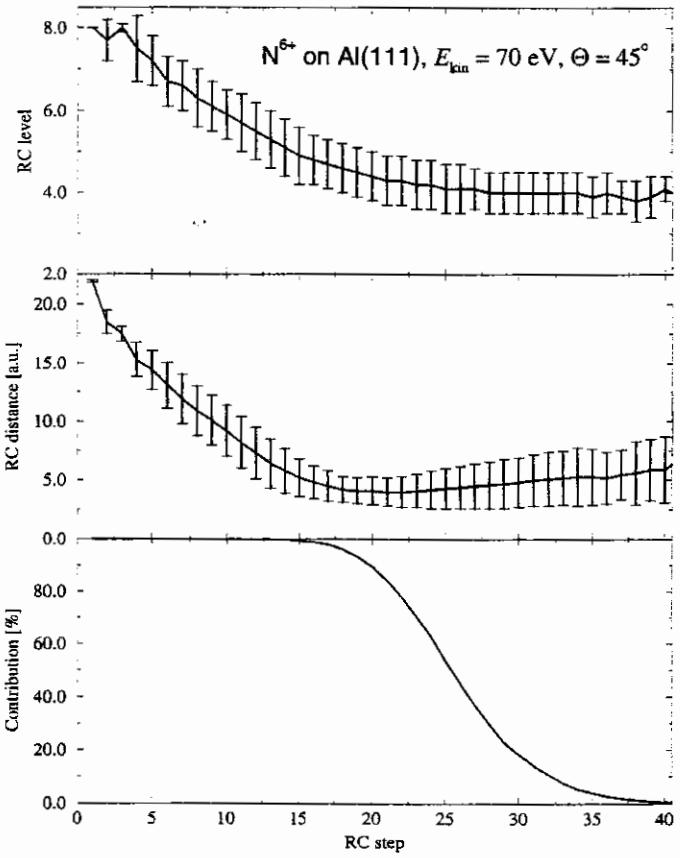

hand, SF is boosted by PO which re-ionizes the HCI and thus allows the formation of a more tightly packed charge cloud.

Within the bulk limit, PO is assumed to occur when the orbital radius $\langle r\rangle_n = n/\sqrt{2E_n}$ exceeds the Thomas–Fermi screening length λ_s (0.92 a.u. for Al and 1.11 a.u. for Au). For the region near and above the jellium edge, we scaled λ_s linearly with the distance R from the first lattice layer and designed a PO rate $\Gamma_{PO}(R)$ which guarantees immediate and vanishing PO in the bulk and asymptotic limit, respectively. The total PO frequency $\Gamma_{PO}(R)$ for finite R is given by the product of the level occupation a_n, the inverse of the time the electron spends in a Bohr orbital above the jellium edge (located at z_j), and the fraction of the orbital volume overlapping with the jellium. From our first attempts to enforce PO as soon as $\langle r\rangle_n > R - z_j$ is realized, we learned that the *delay* introduced in Γ_{PO} is needed to avoid the instant loss of resonantly captured electrons. In Fig. 2, the time evolution of PO for N^{6+} impinging on Al(111) at $E_{kin} = 70$ eV and $\Theta = 45°$ can be followed.

In our simulation, SF has been incorporated via XCV Auger processes ($X \in \{K, L, M, \ldots\}$). The energy released while a charge cloud electron (C) fills an X-shell vacancy generates a valence band (V) excitation. We adopted the tabulated rates $\Gamma_{SF,L}$ for the filling of the L-shell inside the bulk region [14] and extrapolated them towards the vacuum with an exponential decay. As opposed to [15], the decay length for $\Gamma_{SF,L}$ is taken as $\langle r\rangle_n$ and all shells satisfying $\langle r\rangle_n < \lambda_s$ are considered for SF. In order to account for the trend that XCV rates strongly vary with the energy gap between E_n and the valence band [16], the charge cloud content matching the projectile charge q, and the number of vacancies v_n, we applied an additional scaling factor $\propto q v_n/(n_{VB} - n)^{3.46}$ to the base rate $\Gamma^0_{SF,L}$ evaluated at $a_L = 0$. $n_{VB} - 1$ denotes the highest localized atomic level. Fig. 3 shows the subsequent SF steps along the trajectory.

The results of our simulation can be compared with several observables: Our average projectile energy gain of 18.7 eV for N^{6+} comes close to the 16.2 eV measured in [17] for grazing incidence. Our total electron yield of 5.4 electrons for emission in the upper 2π–hemisphere falls within the error bars of recent measurements [18,19]. The simulated secondary electron spectra (not shown) exhibit the same intensity and structures in the low-energy regime as a previous experiment [19]. Looking at simulated final charge distributions, we find that the majority of reflected projectiles is neutral. However, the simulated percentage of about 40% ionized particles long after reflection clearly exceeds the measured values [12]. This discrepancy may be due to feeding mechanisms that are not included in our simulation [10].

The average charge transfer of 27.8 electrons (25.3 via RC and 2.5 via SF) towards the HCI is balanced by the loss of 10.4, 4.8, 6.5, and 0.7 electrons due to total Auger emission, RL, PO and CP, respectively and 5.4 electrons remain with the HCI after reflection. We find that the large flux of the electrons into projectile levels is required to achieve agreement with the experimental total Auger yield and final charge state distributions.

In conclusion, our COM calculations provide projectile level populations along the whole reflected trajectory. We modeled PO and SF mechanisms, and we simultaneously

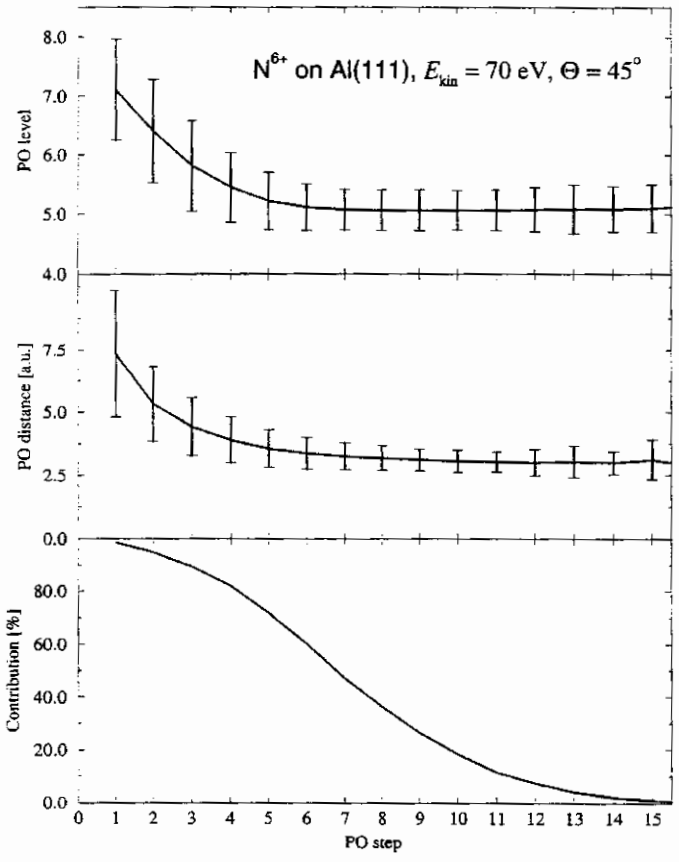

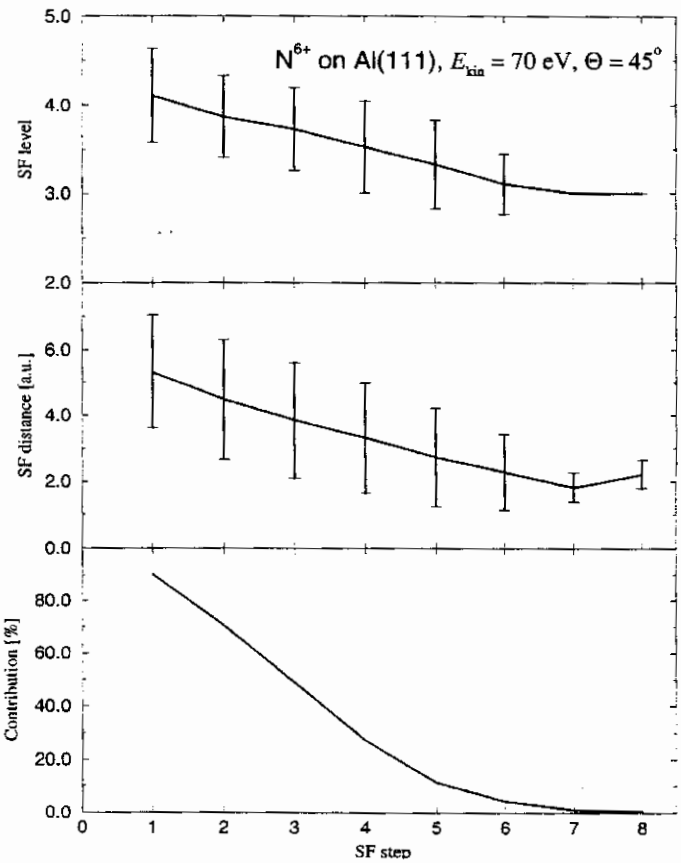

find reasonable agreement with measured projectile charge states, emitted electron yields, and projectile kinetic energy gains.

Acknowledgements

This work was supported by the Division of Chemical Sciences, Basic Energy Sciences, Office of Energy Research, U.S. Department of Energy, by the Kansas Center for Advanced Scientific Computing sponsored by the NSF EPSCoR/K*STAR program, and by the National Science Foundation.

References

1. Arnau, A. *et al.*, Surface Science Reports **27**, 113 (1997).
2. Meyer, F. W. *et al.*, Nucl. Instrum. Methods Phys. Res., Sect. B **125**, 138 (1997).
3. Briand, J. P. *et al.*, Phys. Rev. A **55**, 3947 (1997).
4. Parks, D. C., Bastasz, R., Schmieder, R. W. and Stöckli, M., J. Va. Sci. Technol. B **13**, 941 (1995).
5. Neidhart, T. *et al.*, Physica Scripta **T73**, 307 (1997).
6. Burgdörfer, J., Lerner, P. and Meyer, F. W., Phys. Rev. A **44**, 5674 (1991).
7. Ducrée, J., Casali, F. and Thumm, U., Phys. Rev. A **57**, 338 (1998).
8. Cowan, R. D., "The Theory of Atomic Structure and Spectra" (University of California Press, Berkeley, 1981).
9. Lemell, C. *et al.*, Nucl. Instr. Meth. Phys. Res. Sect. B **102**, 33 (1995).
10. Burgdörfer, J., Reinhold, C. and Meyer, F., Nucl. Instr. Meth. Phys. Res. Sect. B **98**, 415 (1995).
11. Stolterfoht, N., Niemann, D. Grether, M. and Spieler, A. Nucl. Instr. Meth. Phys. Res. Sect. B **124**, 303 (1997).
12. Winecki, S., Cocke, C. L., Fry, D. and Stöckli, M. P., Phys. Rev. A **53**, 1 (1996).
13. Khemliche, H., Limburg, J., Hoekstra, R. and Morgenstern, R., Nucl. Instr. Meth. Phys. Res. Sect. B **125**, 116 (1997).
14. Díez Muiño, R. *et al.*, Phys. Rev. Lett. **76**, 4636 (1996).
15. Thomaschewski, J. *et al.*, Phys. Rev. A **57**, 3665 (1998).
16. Ducrée, J. *et al.*, Phys. Rev. A **57**, 1925 (1998).
17. Winter, H. Auth, C. Schuch, R. and Beebe, E., Phys. Rev. Lett. **71**, 1939 (1993).
18. Eder, H. *et al.*, Physica Scripta **T 73**, 322 (1997).
19. Niemann, D. *et al.*, Phys. Rev. A **56**, 4774 (1997).